AAS 15-585

EFFICIENT MANEUVER PLACEMENT FOR AUTOMATED TRAJECTORY DESIGN

Damon Landau*

When designing a mission, the addition of a maneuver at the right spot often improves the utility of an otherwise mediocre trajectory. However, the additional degrees of freedom of finding the best maneuver location can severely complicate automated broad-search algorithms. A computationally-efficient formulation that reduces the maneuver design space to a single dimension is presented, where the efficacy of additional maneuvers along previously computed transfers is calculated explicitly via Lawden's "primer vector." Examples include leveraging maneuvers to ease capture at Europa, phasing maneuvers to enable resonant-hopping among Saturn's moons, and broken-plane maneuvers on transfers to Mars.

INTRODUCTION

There are many rules of thumb for how to design a trajectory to achieve a set of mission objectives: for example, it's usually efficient to change energy at periapsis, leverage V_∞ at apoapsis, or rendezvous at a node. While such strategies are useful to piece together a design, the best way to solve a mission design problem is generally not known a priori. When the best approach is not apparent, a search of the design space can fill in the gaps for which trajectories can solve the problem at hand. Ideally, the mission designer would not have to artificially restrict the search by presupposing elements of the design, such as when or how to apply a maneuver. (After all the premise of needing a broad search is that the designer doesn't know the right solution.) The search algorithm should not only tap into unknown solutions, but also accommodate previously unknown design problems because each new mission comes with a distinctive set of objectives and constraints. The benefit of this type of general approach is that less time is required to set up new problems and more of the trade space can be explored in an automated fashion, ultimately leading to quicker turn-around and better decision making when designing a trajectory.

The cost of this type of search is additional computation time compared to more specialized approaches, and inefficiencies in any single element can bog down the entire design process. For example, the construction of individual trajectory legs is inherently a two dimensional search (e.g. initial and final time with positions from ephemerides or period and V_∞ for resonances) and can be constructed relatively quickly. However, the addition of a maneuver introduces four additional degrees of freedom (e.g. position and time of the maneuver) and can make the general design problem intractable. One approach is to reduce the degrees of freedom by pre-supposing how and where to perform the maneuver (e.g. tangentially at an apse), but such specialized approaches

*Mission Formulation Engineer, Systems Engineering Section, Jet Propulsion Laboratory, California Institute of Technology, 4800 Oak Grove Dr., Pasadena, CA, 91109

© 2015 California Institute of Technology. Government sponsorship acknowledged.

only work for specialized problems. Moreover, the designer is forced to come up with different maneuver strategies each time the mission objectives change. When the design problem calls for a broad search of a broad set of mission objectives, a different approach is warranted.

With these design principles in mind, a maneuver placement algorithm is constructed to augment broad search strategies where the encounter times are pre-specified search parameters and the orbital transfers are solutions to Lambert's problem.[1–3] The resulting conics are patched with a ΔV at (powered) flybys or with departure and arrival maneuvers for rendezvous. In this way each individual leg can be computed independent of all the other transfers, which tends to reduce the total number of trajectory calculations.[1,2] However, the only place for maneuvers in this scenario are at the flybys, which tend to be unfavorable for optimal trajectories. It is therefore desirable to find locations on the conic arcs that are favorable to achieve some objective. For example the objective would be lower the arrival V-infinity for leveraging, reduce the size of the orbit to reach the inner moons of a planetary system, or minimize inclination for broken-plane maneuvers. Due to the specific broad search setup, the effect of any individual maneuver on the entire trajectory is not known but locally optimal improvements can be made to produce the desired results when the entire trajectory is pieced together. The trade space of trajectories is increased by sampling a range of maneuver magnitudes, which has the additional benefit of only computing transfers with acceptable ΔV.

OPTIMAL MANEUVER PLACEMENT

Optimality Conditions

The optimization problem then becomes to minimize an arbitrary performance index

$$J\left(\mathbf{v}_0, \mathbf{v}_f, \Delta V_{con}\right) \tag{1}$$

subject to fixed initial and final positions and a ΔV magnitude constraint.

$$\begin{aligned} &\mathbf{r}_0 = \mathbf{r}_{0,con},\ \mathbf{r}_f = \mathbf{r}_{f,con} \\ &\Delta V = \Delta V_{con} \end{aligned} \tag{2}$$

Note that J does not depend on the time or position at the beginning and end of the transfer leg (Lambert arc) because the time is pre-specified for the broad search and the position depends on the body ephemeris. This constrained optimization problem is readily addressed using Lagrange's method where the objective is augmented with the constraints using Lagrange multipliers $\boldsymbol{\lambda}$ and μ.

$$\begin{aligned} L = J &+ \mu_{\mathbf{r}_0}\left(\mathbf{r}_0 - \mathbf{r}_{0,con}\right) + \mu_{\mathbf{r}_f}\left(\mathbf{r}_f - \mathbf{r}_{f,con}\right) \\ &+ \mu_{\Delta V}\left(\int_{t_0}^{t_f} \sqrt{\mathbf{a}^T\mathbf{a}}\,dt - \Delta V_{con}\right) + \int_{t_0}^{t_f} \boldsymbol{\lambda}^T\left(\ddot{\mathbf{r}} - \mathbf{g}(\mathbf{r}) - \mathbf{a}\right)dt \end{aligned} \tag{3}$$

The time varying multiplier $\boldsymbol{\lambda}$ accounts for the sensitivity to the equations of motion

$$\ddot{\mathbf{r}} = \mathbf{g}(\mathbf{r}) + \mathbf{a} \tag{4}$$

where $\mathbf{g}(\mathbf{r})$ is the acceleration due to gravity and $\mathbf{a}$ is the control acceleration (due to thrust). The ΔV magnitude constraint Eq. (2) is made into a function of $\mathbf{a}$ via Eq. (5)

$$\Delta V = \int_{t_0}^{t_f} \sqrt{\mathbf{a}^T\mathbf{a}}\,dt \tag{5}$$

The optimum conditions to minimize J are now found by setting the variation in L to zero (where $L = J$ when the constraints are met). First Eq. (3) is rearranged by integrating $\boldsymbol{\lambda}^T\ddot{\mathbf{r}}$ by parts twice, where $\mathbf{v} \equiv \dot{\mathbf{r}}$.

$$L = J - \mu_{\Delta V}\Delta V_{con} + \mu_{\mathbf{r}_0}\left(\mathbf{r}_0 - \mathbf{r}_{0,con}\right) + \mu_{\mathbf{r}_f}\left(\mathbf{r}_f - \mathbf{r}_{f,con}\right)$$
$$+\boldsymbol{\lambda}_f^T\mathbf{v}_f - \boldsymbol{\lambda}_0^T\mathbf{v}_0 - \dot{\boldsymbol{\lambda}}_f^T\mathbf{r}_f + \dot{\boldsymbol{\lambda}}_0^T\mathbf{r}_0 + \int_{t_0}^{t_f}\left(\mu_{\Delta V}\sqrt{\mathbf{a}^T\mathbf{a}} + \ddot{\boldsymbol{\lambda}}^T\mathbf{r} - \boldsymbol{\lambda}^T\mathbf{g} - \boldsymbol{\lambda}^T\mathbf{a}\right)dt \tag{6}$$

Variations due to $\mathbf{r}_0$ and $\mathbf{r}_f$ are trivially zero since they are fixed.

$$\frac{\partial L}{\partial \mathbf{r}_0} = \mathbf{0} = \mu_{\mathbf{r}_0} + \dot{\boldsymbol{\lambda}}_0 \rightarrow \mu_{\mathbf{r}_0} = -\dot{\boldsymbol{\lambda}}_0$$
$$\frac{\partial L}{\partial \mathbf{r}_f} = \mathbf{0} = \mu_{\mathbf{r}_f} - \dot{\boldsymbol{\lambda}}_f \rightarrow \mu_{\mathbf{r}_f} = \dot{\boldsymbol{\lambda}}_f \tag{7}$$

The variation due to $\mathbf{v}_0$ and $\mathbf{v}_f$ provide boundary conditions on $\boldsymbol{\lambda}$

$$\frac{\partial L}{\partial \mathbf{v}_0} = \mathbf{0} = \frac{\partial J}{\partial \mathbf{v}_0} - \boldsymbol{\lambda}\left(t_0\right) \rightarrow \boldsymbol{\lambda}\left(t_0\right) = \frac{\partial J}{\partial \mathbf{v}_0}$$
$$\frac{\partial L}{\partial \mathbf{v}_f} = \mathbf{0} = \frac{\partial J}{\partial \mathbf{v}_f} + \boldsymbol{\lambda}\left(t_f\right) \rightarrow \boldsymbol{\lambda}\left(t_f\right) = -\frac{\partial J}{\partial \mathbf{v}_f} \tag{8}$$

The variation due to $\mathbf{r}$ provides the equations of motion for $\boldsymbol{\lambda}$

$$\frac{\partial L}{\partial \mathbf{r}} = \mathbf{0} = \int_{t_0}^{t_f}\left(\ddot{\boldsymbol{\lambda}}^T - \boldsymbol{\lambda}^T\frac{\partial \mathbf{g}}{\partial \mathbf{r}}\right)dt \rightarrow \ddot{\boldsymbol{\lambda}}^T = \boldsymbol{\lambda}^T\frac{\partial \mathbf{g}}{\partial \mathbf{r}} \tag{9}$$

Thus the behavior of $\boldsymbol{\lambda}$ is completely determined by $\partial J/\partial \mathbf{v}_0$, $\partial J/\partial \mathbf{v}_f$, and $\partial \mathbf{g}/\partial \mathbf{r}$.

Suppose that the thrust begins at maneuver time t_m, is finite over the interval Δt, and is constrained to zero otherwise. The variation due to $\mathbf{a}$ provides the control law during this interval. From Eq. (10) the acceleration should be aligned with $\boldsymbol{\lambda}$.

$$\frac{\partial L}{\partial \mathbf{a}} = \mathbf{0} = \int_{t_m}^{t_m+\Delta t}\left(\mu_{\Delta V}\hat{\mathbf{a}} - \boldsymbol{\lambda}\right)dt \rightarrow \hat{\mathbf{a}} = \hat{\boldsymbol{\lambda}} \tag{10}$$

The original optimization problem of finding the largest decrease in J for a given ΔV constraint provides guidance on when to thrust. From Eq. (11) the thrust profile that maximizes $\mu_{\Delta V}$ achieves the greatest reduction in L with limited ΔV.

$$\delta L = \frac{\partial L}{\partial \Delta V_{con}}\delta\Delta V_{con} = \left(\frac{\partial J}{\partial \Delta V_{con}} - \mu_{\Delta V}\right)\delta\Delta V_{con} \tag{11}$$

Moreover it is only beneficial to thrust when $\mu_{\Delta V} > \partial J/\partial \Delta V_{con}$. (The optimal unconstrained value for ΔV_{con} could also be found by setting Eq. (11) to zero.) From Eq. (10)

$$\mathbf{0} = \int_{t_m}^{t_m+\Delta t}\left(\mu_{\Delta V}\hat{\mathbf{a}} - \boldsymbol{\lambda}\right)dt \rightarrow \int_{t_m}^{t_m+\Delta t}\mu_{\Delta V}\hat{\mathbf{a}}dt = \int_{t_m}^{t_m+\Delta t}\boldsymbol{\lambda}dt = \int_{t_m}^{t_m+\Delta t}\lambda\hat{\mathbf{a}}dt$$
$$\int_{t_m}^{t_m+\Delta t}\mu_{\Delta V}\hat{\mathbf{a}}dt = \int_{t_m}^{t_m+\Delta t}\lambda\hat{\mathbf{a}}dt \rightarrow \int_{t_m}^{t_m+\Delta t}\mu_{\Delta V}dt = \int_{t_m}^{t_m+\Delta t}\lambda dt \rightarrow \mu_{\Delta V} = \frac{1}{\Delta t}\int_{t_m}^{t_m+\Delta t}\lambda dt \tag{12}$$

so that $\mu_{\Delta V}$ is the average value for $\lambda = \left|\boldsymbol{\lambda}\right|$ while thrusting. It is therefore optimal to thrust only at the time when λ_v is largest. For an impulsive thrust

$$\mu_{\Delta V} = \lambda\left(t_m\right) \tag{13}$$

and the problem of minimizing L (which from Eq. (3) minimizes J when the constraints are met) is transformed to the problem of finding the time when λ_v is maximum.

Analytic Solution

The solution to $\lambda_v(t)$ begins with Eq. (9) and noting

$$\ddot{\boldsymbol{\lambda}}^T = \boldsymbol{\lambda}^T \frac{\partial \mathbf{g}}{\partial \mathbf{r}} \rightarrow \ddot{\boldsymbol{\lambda}} = \frac{\partial \mathbf{g}}{\partial \mathbf{r}} \boldsymbol{\lambda} \tag{14}$$

since $\partial \mathbf{g}/\partial \mathbf{r} = \left[\partial \mathbf{g}/\partial \mathbf{r}\right]^T$ for gravity derivable from a potential. Equation (14) has the same form of the variational equations due to linearization of the state equations of motion (Eqs. (4)), which fortunately has an analytic solution for conics. Lawden[4] denoted $\boldsymbol{\lambda}$ as the primer vector **P**, and provided a solution in radial-tangential-normal coordinates as

$$\mathbf{P} = \begin{bmatrix} P_R \\ P_T \\ P_N \end{bmatrix} = \begin{bmatrix} A\cos\nu - Be\sin\nu + CI_1 \\ -A\sin\nu + B(1+e\cos\nu) + \dfrac{D - A\sin\nu}{1+e\cos\nu} + CI_2 \\ (E\cos\nu + F\sin\nu)/(1+e\cos\nu) \end{bmatrix} \tag{15}$$

where e is the (constant) eccentricity of the transfer, and ν is the true anomaly (varies with time). Lawden gave a solution for I_1 and I_2 in Ref 6, but the more convenient form of Eq. (16) can be found in Ref 5, where M is the mean anomaly along the orbit. (And a historical perspective of this equation is discussed in Ref 7.) Equation (16) remains real and valid for $e > 1$ even though M and $\sqrt{1-e^2}$ to become imaginary, or an alternate form for hyperbolic transfers can be found in Ref 5. When the eccentricity is numerically close to one, the parabolic form of Eq. (17) is sufficient to place the maneuver.

$$\begin{aligned} I_1 &= \frac{1}{1-e^2}\left[\frac{2e}{1+e\cos\nu} - \cos\nu - \frac{3e^2 M\sin\nu}{\left(1-e^2\right)^{3/2}}\right] \\ I_2 &= \frac{1}{1-e^2}\left[\left(1+\frac{1}{1+e\cos\nu}\right)\sin\nu - \frac{3eM(1+e\cos\nu)}{\left(1-e^2\right)^{3/2}}\right] \end{aligned} \tag{16}$$

$$\begin{aligned} I_1\big|_{e=1} &= \tfrac{1}{2}\sin\nu\left(\tan\tfrac{\nu}{2} - \tfrac{1}{5}\tan^5\tfrac{\nu}{2}\right) - \cos\nu/(1+\cos\nu)^2 \\ I_2\big|_{e=1} &= \tfrac{1}{2}(1+\cos\nu)\left(\tan\tfrac{\nu}{2} - \tfrac{1}{5}\tan^5\tfrac{\nu}{2}\right) \end{aligned} \tag{17}$$

The remaining constants in *A, B, C, D, E, F* are solved by constraining the endpoints to Eq. (8), and noting that the out-of-plane motion is decoupled.

$$\begin{bmatrix} \cos\nu_0 & -e\sin\nu_0 & I_1(t_0) & 0 \\ -(1+r_0/p)\sin\nu_0 & p/r_0 & I_2(t_0) & r_0/p \\ \cos\nu_f & -e\sin\nu_f 0 & I_1(t_f) & 0 \\ -(1+r_f/p)\sin\nu_f & p/r_f & I_2(t_f) & r_f/p \end{bmatrix} \begin{bmatrix} A \\ B \\ C \\ D \end{bmatrix} = \begin{bmatrix} \frac{\partial J}{\partial V_{R0}} \\ \frac{\partial J}{\partial V_{T0}} \\ -\frac{\partial J}{\partial V_{Rf}} \\ -\frac{\partial J}{\partial V_{Tf}} \end{bmatrix} \tag{18}$$

$$\begin{bmatrix} r_0/p\cos\nu_0 & r_0/p\sin\nu_0 \\ r_f/p\cos\nu_f & r_f/p\sin\nu_f \end{bmatrix} \begin{bmatrix} E \\ F \end{bmatrix} = \begin{bmatrix} \frac{\partial J}{\partial V_{N0}} \\ -\frac{\partial J}{\partial V_{Nf}} \end{bmatrix}$$

with

$$r/p = 1/(1+e\cos\nu) \tag{19}$$

The first and second derivatives are efficiently computed with Eqs. (20), and improve convergence in most optimization algorithms when maximizing the magnitude of **P**. There are typically multiple local maxima, especially on transfers with multiple revolutions, so it is recommended to run multiple optimizations using periapsis and apoapsis on each revolution as an initial guess. The mid-angle point makes a suitable starting point on transfers that do not pass through an apse.

$$\begin{aligned}
\mathbf{P}' &= \frac{\partial \mathbf{P}}{\partial \nu} = \begin{bmatrix} P_T(1-r/p) - (A\sin\nu - C\sin\nu + De\cos\nu)(r/p)^2 \\ (Ae + P_T e\sin\nu + De\cos\nu)(r/p) - 2P_R \\ (-E\sin\nu + eF + F\cos\nu)(r/p)^2 \end{bmatrix} \\
\mathbf{P}'' &= \frac{\partial \mathbf{P}'}{\partial \nu} = \begin{bmatrix} 2eC(r/p)^3 - P_R \\ P_T(1-r/p) + 2e\sin\nu(P_T' + P_R)(r/p) - 2P_R' \\ (2eP_N'\sin\nu - P_N)(r/p) \end{bmatrix}
\end{aligned} \tag{20}$$

The process of determining the best time and direction of the maneuver is computationally efficient because the primer vector mapping is an explicit function of only the true anomaly. In this way an arbitrary objective J can be included without pre-supposing the maneuver time or direction as in Refs 3,8, and 9. Moreover, the algorithm is not constrained to transfers between circular orbits or even to the same body.

EFFICIENT MANEUVER MODEL

In general, the addition of a maneuver introduces four degrees of freedom to the problem of connecting position $\mathbf{R}_0$ at time t_0 to position $\mathbf{R}_f$ at time t_f, and the additional search parameters could render many broad-search algorithms impractical. The primer vector analysis essentially reduces this four-dimensional problem to two one-dimensional searches conducted in sequence. First the optimal true anomaly of the maneuver is determined by maximizing the magnitude of the primer vector over the ballistic transfer. Then two additional degrees of freedom are immediately available from the primer unit vector to specify the maneuver direction. By assuming that the first-order-optimal maneuver location and direction remain effective with non-infinitesimal maneuvers, only one additional search dimension is introduced to the broad search problem. Noting that it is usually desirable to bound the total mission ΔV, the maneuver magnitude becomes a convenient search parameter.

Ideally, the resulting initial and final velocities could be directly computed from the initial and final positions and times, along with the maneuver true anomaly and ΔV. Unfortunately, (to the chagrin of anyone who's dealt with Lambert's problem) the time of flight equation cannot be solved explicitly and an iterative procedure is required. Fortunately, the solution of flight time with an intermediate maneuver can be reduced to a single search parameter (Similar to Lambert's problem) by explicitly solving for the **ΔV** vector. The solution for the transfer begins with the classic F and G functions[10] as specified in Eqs. (21).

$$
\begin{aligned}
&\mathbf{R}_f = F\mathbf{R}_0 + G\mathbf{V}_0,\ \mathbf{R}_0 = \dot{G}\mathbf{R}_f - G\mathbf{V}_f \\
&F = 1 - \frac{r_f}{p}\left(1-\cos\theta_{0f}\right),\ G = \frac{r_0 r_f}{\sqrt{\mu p}}\sin\theta_{0f},\ \dot{G} = 1 - \frac{r_0}{p}\left(1-\cos\theta_{0f}\right) \\
&\theta_{0f} = \nu_f - \nu_0
\end{aligned}
\tag{21}
$$

An expression for the initial and final velocities is then readily available.

$$
\begin{aligned}
\mathbf{V}_0 &= \frac{\sqrt{\mu p}}{r_0 r_f \sin\theta_{0f}}\left[\mathbf{R}_f - \mathbf{R}_0 + \frac{r_f}{p}\left(1-\cos\theta_{0f}\right)\mathbf{R}_0\right] \\
\mathbf{V}_f &= \frac{\sqrt{\mu p}}{r_0 r_f \sin\theta_{0f}}\left[\mathbf{R}_f - \mathbf{R}_0 - \frac{r_0}{p}\left(1-\cos\theta_{0f}\right)\mathbf{R}_f\right]
\end{aligned}
\tag{22}
$$

Equations (22) are general for any conic arc. For the present problem the subscripts 1 and 2 are introduced to specify the first (preceding the maneuver $\mathbf{R}_m$) and second (following the maneuver) conic arcs that patch $\mathbf{R}_0$ to $\mathbf{R}_f$ in the original ballistic transfer. The maneuver $\mathbf{\Delta V}$ vector is then the difference between the velocity at the beginning of the second arc and the velocity at the end of the first arc, where the relation $p = r^2 V_T^2 / \mu$ is applied in Eq. (23).

$$
\begin{aligned}
\mathbf{\Delta V} &= \mathbf{V}_{02} - \mathbf{V}_{f1} \\
&= \frac{\sqrt{\mu p_f}}{r_m r_f \sin\theta_{mf}}\left[\mathbf{R}_f - \mathbf{R}_m + \frac{r_f}{p_f}\left(1-\cos\theta_{mf}\right)\mathbf{R}_m\right] \\
&\quad - \frac{\sqrt{\mu p_0}}{r_0 r_m \sin\theta_{0m}}\left[\mathbf{R}_m - \mathbf{R}_0 - \frac{r_0}{p_0}\left(1-\cos\theta_{0m}\right)\mathbf{R}_m\right] \\
&= \frac{V_{T2}}{\sin\theta_{mf}}\left[\hat{\mathbf{R}}_f - \frac{r_m}{r_f}\hat{\mathbf{R}}_m + \frac{\mu}{r_m V_{T2}^2}\left(1-\cos\theta_{mf}\right)\hat{\mathbf{R}}_m\right] \\
&\quad - \frac{V_{T1}}{\sin\theta_{0m}}\left[\frac{r_m}{r_0}\hat{\mathbf{R}}_m - \hat{\mathbf{R}}_0 - \frac{\mu}{r_m V_{T1}^2}\left(1-\cos\theta_{0m}\right)\hat{\mathbf{R}}_m\right]
\end{aligned}
\tag{23}
$$

The position vectors are expressed in the RTN frame of the maneuver (notably the same frame from the primer vector analysis) in Eq. (24) by employing the geometry specified in Figure 1. The tangential and normal directions are defined so that $\hat{\mathbf{T}}_m$ is in the plane created by $\mathbf{R}_0$ and $\mathbf{R}_m$.

$$
\begin{aligned}
&\hat{\mathbf{R}}_0 = \begin{bmatrix} \cos\theta_{0m} \\ -\sin\theta_{0m} \\ 0 \end{bmatrix},\ \hat{\mathbf{R}}_m = \begin{bmatrix} 1 \\ 0 \\ 0 \end{bmatrix} \\
&\hat{\mathbf{R}}_f = \begin{bmatrix} \cos\theta_{0f}\cos\theta_{0m} + \sin\theta_{0f}\sin\theta_{0m}\cos i_0 \\ \sin\theta_{0f}\cos\theta_{0m}\cos i_0 - \cos\theta_{0f}\sin\theta_{0m} \\ -\sin\theta_{0f}\sin i_0 \end{bmatrix}
\end{aligned}
\tag{24}
$$

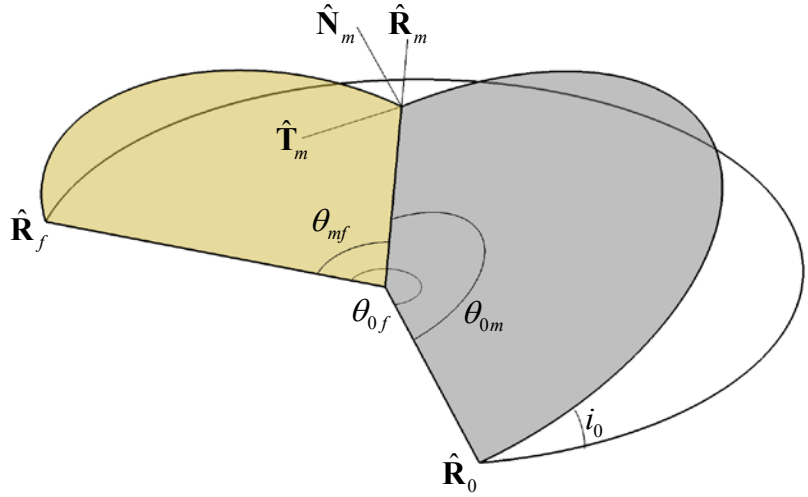

Figure 1 The maneuver location $\hat{\mathbf{R}}_m$ is determined by a transfer angle θ_{0m} from the initial position $\hat{\mathbf{R}}_0$ and an inclination of i_0 from the plane created by the original ballistic transfer.

The **ΔV** vector can now be expressed in RTN coordinates as Eqs. (25)–(27).

$$\Delta V_R = -\frac{r_m V_{T1}}{r_0 \sin\theta_{0m}} - \frac{r_m V_{T2}}{r_f \sin\theta_{mf}} + \frac{V_{T1}}{\tan\theta_{0m}} + \frac{V_{T2}}{\tan\theta_{mf}} + \frac{\mu}{r_m V_{T1}} \tan\frac{\theta_{0m}}{2} + \frac{\mu}{r_m V_{T2}} \tan\frac{\theta_{mf}}{2} \tag{25}$$

$$\Delta V_T = \frac{V_{T2}}{\sin\theta_{mf}} \left(\sin\theta_{0f} \cos\theta_{0m} \cos i_0 - \cos\theta_{0f} \sin\theta_{0m} \right) - V_{T1} \tag{26}$$

$$\Delta V_N = -\frac{V_{T2}}{\sin\theta_{mf}} \sin\theta_{0f} \sin i_0 \tag{27}$$

The initial and final position vectors on the transfer provide r_0, r_f, θ_{0f}, while the primer vector analysis establishes $\Delta V_R, \Delta V_T, \Delta V_N, \theta_{0m}$, leaving $V_{T1}, V_{T2}, r_m, \theta_{mf}, i_0$ to be determined. The geometry of the transfer constrains the relation between θ_{mf} and i_0 according to Eq. (28).

$$\cos\theta_{mf} = \hat{\mathbf{R}}_m \square \hat{\mathbf{R}}_f = \cos\theta_{0f} \cos\theta_{0m} + \sin\theta_{0f} \sin\theta_{0m} \cos i_0 \tag{28}$$

An additional constraint arises from requiring that the sum of flight times before and after the maneuver equal the flight time on the original transfer.

$$t_{0f} = t_{0m} + t_{mf} \tag{29}$$

Because the flight time on a conic (Kepler's equation) is transcendental an iterative procedure is required. By choosing V_{T1} as the independent parameter, equations (25)–(28) can be solved algebraically, providing a straightforward calculation of the total flight time as follows:

First, combine (26) and (27) to eliminate $V_{T2}/\sin\theta_{mf}$ and solve for i_0

$$\left[\Delta V_N \sin\theta_{0f} \cos\theta_{0m}\right] \cos i_0 + \left[\left(\Delta V_T + V_{T1}\right) \sin\theta_{0f}\right] \sin i_0 = \Delta V_N \cos\theta_{0f} \sin\theta_{0m}$$

$$i_0 = \pm\cos^{-1}\left(\frac{\Delta V_N \cos\theta_{0f} \sin\theta_{0m}}{x \sin\theta_{0f}}\right) + 2\tan^{-1}\left(\frac{x - \Delta V_N \cos\theta_{0m}}{\Delta V_T + V_{T1}}\right) \tag{30}$$

where $x=\sqrt{\left(\Delta V_N \cos\theta_{0m}\right)^2+\left(\Delta V_T+V_{T1}\right)^2}$. The sign ambiguity in the expression for i_0 is resolved by choosing the solution that is closest to the plane of the initial transfer (e.g. maximum $\cos i_0$). Now equations (26) and (28) are combined to solve V_{T2}.

$$\sin\theta_{mf}=\pm\sqrt{1-\cos^2\theta_{mf}}=\pm\sqrt{1-\left(\cos\theta_{0f}\cos\theta_{0m}+\sin\theta_{0f}\sin\theta_{0m}\cos i_0\right)^2} \tag{31}$$

$$V_{T2}=\frac{\left(V_{T1}+\Delta V_T\right)\sin\theta_{mf}}{\sin\theta_{0f}\cos\theta_{0m}\cos i_0-\cos\theta_{0f}\sin\theta_{0m}} \tag{32}$$

The choice of sign in Eq. (31) is resolved by requiring $V_{T2}>0$. The radius of the maneuver location can be found by rearranging Eq. (25) into (33) and solving by quadratic formula. The sign ambiguity is resolved by requiring $r_m>0$. If both solutions are positive, then the option that is closest to the radius from the previous iteration is selected (where the ballistic solution provides an initial seed).

$$-\left(\frac{r_m V_{T1}}{r_0\sin\theta_{0m}}+\frac{r_m V_{T2}}{r_f\sin\theta_{mf}}\right)r_m^2+\left(\frac{V_{T1}}{\tan\theta_{0m}}+\frac{V_{T2}}{\tan\theta_{mf}}-\Delta V_R\right)r_m+\left(\frac{\mu}{V_{T1}}\tan\tfrac{\theta_{0m}}{2}+\frac{\mu}{V_{T2}}\tan\tfrac{\theta_{mf}}{2}\right)=0 \tag{33}$$

The position vector of a maneuver that provides the desired $\mathbf{\Delta V}$ vector is calculated from r_m, θ_{0m}, and i_0 in the local RTN frame of $\mathbf{R}_0$ via Eq. (34) (where the normal direction is defined by the plane of the original ballistic transfer, and different than the maneuver RTN frame).

$$\mathbf{R}_m=r_m\begin{bmatrix}\cos\theta_{0m}\\ \sin\theta_{0m}\cos i_0\\ \sin\theta_{0m}\sin i_0\end{bmatrix} \tag{34}$$

In order to explicitly solve for the desired $\mathbf{\Delta V}$, the angle from the initial position θ_{0m} out of the primer vector analysis is held constant, which results in a change from the optimal true anomaly ν_m found from maximizing the primer vector magnitude. However, the optimal true anomaly also changes from the first-order analysis for different values of the maneuver magnitude. Thus as the ΔV increases the maneuver position and direction are likely to stray farther from optimal, but still remain an effective first guess for later optimization.

With the geometry of the transfer completely specified, the calculation of flight time begins by finding the radial velocity components at the initial and maneuver times.

$$\begin{aligned}V_{R0}&=-\frac{V_{T1}}{\sin\theta_{0m}}+\frac{h_1}{r_0\tan\theta_{0m}}+\frac{\mu}{h_1}\tan\tfrac{\theta_{0m}}{2}\\ V_{R1}&=\frac{h_1}{r_1\sin\theta_{0m}}-\frac{V_{T1}}{\tan\theta_{0m}}-\frac{\mu}{h_1}\tan\tfrac{\theta_{0m}}{2}\end{aligned} \tag{35}$$

where $h_1=r_m V_{T1}$. Next, a parameter proportional to energy is specified in Eq. (36) and an intermediate anomaly related to Sundman's anomaly[10] is calculated via Eq. (37).

$$\alpha_1=2\mu/r_0-V_{R0}^2-h_1^2/r_0^2 \tag{36}$$

$$\chi_1=\frac{2}{\sqrt{\alpha_1}}\tan^{-1}\left(\frac{\sqrt{\alpha_1}\,r_0\tan\frac{\theta_{0m}}{2}}{h_1-V_{R0}r_0\tan\frac{\theta_{0m}}{2}}\right) \tag{37}$$

The flight time on the first arc is found with Eq. (38).

$$t_{0m}=\left(\mu\chi_1+V_{R0}r_0-V_{R1}r_m\right)/\alpha_1+N_1\mu/\sqrt{\alpha_1^3} \tag{38}$$

It is noteworthy that χ_1 always takes on real values even for $\alpha_1 < 0$, thus the difference between elliptic and hyperbolic orbits is transparent for programs that allow inverse tangent to become imaginary. Alternatively in the hyperbolic case, the inverse hyperbolic tangent could be employed with $\sqrt{-\alpha_1}$ to keep it real. The last term in Eq. (38) arises because the elliptic case can take on additional revolutions. In the case of a nearly parabolic arc α approaches zero and Eq. (38) becomes numerically unstable. In applications where a high degree of accuracy is warranted, a series solution is recommended (several options can be found in Ref 10). However, in the context of a broad search a small error can be incurred by using the equation of time for an exact parabola when the eccentricity is numerically close to one. The small error in time translates to a small error in $\mathbf{\Delta V}$ when the results of the broad search are transferred to a higher fidelity model.

$$N_1 = \begin{cases} \lfloor \theta_{0m}/2\pi \rfloor & \alpha_1 > 0 \,\&\, \chi_1 > 0 \\ \lfloor \theta_{0m}/2\pi \rfloor + 1 & \alpha_1 > 0 \,\&\, \chi_1 < 0 \\ 0 & \alpha_1 < 0 \end{cases} \tag{39}$$

Similarly the flight time on the second arc (following the maneuver) is found with Eqs. (40)-(44).

$$V_{Rf} = \frac{V_{T2}}{\sin\theta_{mf}} - \frac{h_2}{r_f \tan\theta_{mf}} - \frac{\mu}{h_2}\tan\frac{\theta_{mf}}{2} \tag{40}$$

$$\alpha_2 = 2\mu/r_f - V_{Rf}^2 - h_f^2/r_f^2 \tag{41}$$

$$\chi_2 = \frac{2}{\sqrt{\alpha_2}}\tan^{-1}\left(\frac{\sqrt{\alpha_2}\, r_f \tan\frac{\theta_{mf}}{2}}{h_2 + V_{Rf} r_f \tan\frac{\theta_{mf}}{2}}\right) \tag{42}$$

$$t_{mf} = \left(\mu\chi_2 + \left(V_{R1} + \Delta V_R\right) r_m - V_{Rf} r_f\right)/\alpha_2 + N_2 \mu/\sqrt{\alpha_2^3} \tag{43}$$

$$N_2 = \begin{cases} \lfloor \left(\theta_{0f} - \theta_{0m}\right)/2\pi \rfloor & \alpha_2 > 0 \,\&\, \chi_2 > 0 \\ \lfloor \left(\theta_{0f} - \theta_{0m}\right)/2\pi \rfloor + 1 & \alpha_2 > 0 \,\&\, \chi_2 < 0 \\ 0 & \alpha_2 < 0 \end{cases} \tag{44}$$

The error in the fight time is then corrected by iterating on V_{T1} to some tolerance. In the context of a broad search the acceptable error can be larger (say 10^{-4}) than in other applications because the entire trajectory is assumed to be modified later in a higher fidelity model and computation speed is a relatively higher priority than accuracy when searching over an extremely large number of trajectories. It is also noted that in some cases no solution exists to connect $\mathbf{R}_0$ and $\mathbf{R}_f$ with the specified flight time and ΔV. These cases manifest themselves when there is no real solution to Eqs. (30) or (33) or when the derivative of $t_{0m}+t_{mf}$ with respect to the independent parameter V_{T1} tends towards zero (root-solving algorithms that employ second-order derivatives are particularly adept at locating such cases). When these cases arise the recommended course of action is to incrementally reduce the ΔV magnitude until a solution exists. Because the maneuver is derived from an initially ballistic transfer, a solution is guaranteed to exist for some smaller value of ΔV. Alternatively, these cases can be removed outright when the desired transfer is represented by a previously converged solution at a lower ΔV during the search process.

For transfers that do converge to a solution for flight time, the initial and final velocities are calculated in their local RTN frames via Eqs. (45) and (46). A new value for the objective function is then computed and the solution is kept if there is a net improvement, i.e. if the reduction in J due to V_0 and V_f is greater than the increase due to ΔV.

$$\mathbf{V}_0 = \begin{bmatrix} V_{R0} \\ \cos i_0 h_1 / r_0 \\ \sin i_0 h_1 / r_0 \end{bmatrix} \tag{45}$$

$$\mathbf{V}_f = \begin{bmatrix} V_{Rf} \\ \sqrt{1 - \left(\sin i_0 \sin \theta_{0m} / \sin \theta_{mf}\right)^2}\, h_2 / r_f \\ -\left(\sin i_0 \sin \theta_{0m} / \sin \theta_{mf}\right) h_2 / r_f \end{bmatrix} \tag{46}$$

EXAMPLE MISSIONS

To demonstrate the effectiveness of the primer vector to place maneuvers in a broad search with arbitrary objectives, three examples are examined. First, traditional V_∞ leveraging is employed at the end of a Jovian tour to lower the ΔV to enter into orbit at Europa. Then, a tour of Saturn is examined where the objective on each leg is to provide the greatest change in orbital period (in addition to V_∞) to pass between resonances before entering orbit at Enceladus. Finally, broken-plane transfers from Earth to Mars are examined where the objective is to maximize delivered mass using a fictitious launch vehicle that has a significant penalty for non-zero escape declinations.

Banzai Pipeline to Europa

The parameters for the broad search of the last few transfers of a Jovian tour to Europa are given in Table 1, where the objective for leveraging lowers the end V_∞ and increases the beginning V_∞ to connect to the previous leg. As shown in Eq. (47) the maneuver objective for capture is modified by accounting for the Oberth effect of increased efficiency of capturing at a finite circular radius from a gravitating body. The primer vector over the transfer is then computed from the derivative of J with respect to the $\mathbf{V}_\infty$ vectors using Eq. (18). Figure 2 confirms that it is optimal to perform V_∞ leveraging maneuvers by thrusting tangentially at apoapsis. The effect of different flight times and arrival dates from the broad search are presented in Figure 3, where each dot is a trajectory solution from the broad search. Figure 4 illustrates the effect of the leveraging maneuvers to lower arrival V_∞ in concert with a series of 180° transfers from Callisto and Ganymede.

Table 1. Search parameters to reduce capture ΔV into 100-km circular orbit at Europa

Maneuver Objective	Increase initial and lower final V_∞
Max. maneuver ΔV	200 m/s
Maneuver ΔV increment	10 m/s
Flyby Sequence	CCGGEEE[1]
Arrival date	Jan. 2027–Jan. 2028
Max. flight time per leg	30 d
Max. total flight time	90 d
Time step	0.1 d C&G, 0.03 d E
Max. flyby ΔV	5 m/s
Min. flyby alt.	100 km

[1]C = Callisto, G =Ganymede, E = Europa

$$
\begin{aligned}
J_{leveraging} &= v_{\infty,f} - v_{\infty,0} \\
J_{capture} &= \sqrt{v_{\infty,f}^2 + 2GM/r_{circ}} - v_{\infty,0}
\end{aligned}
\tag{47}
$$

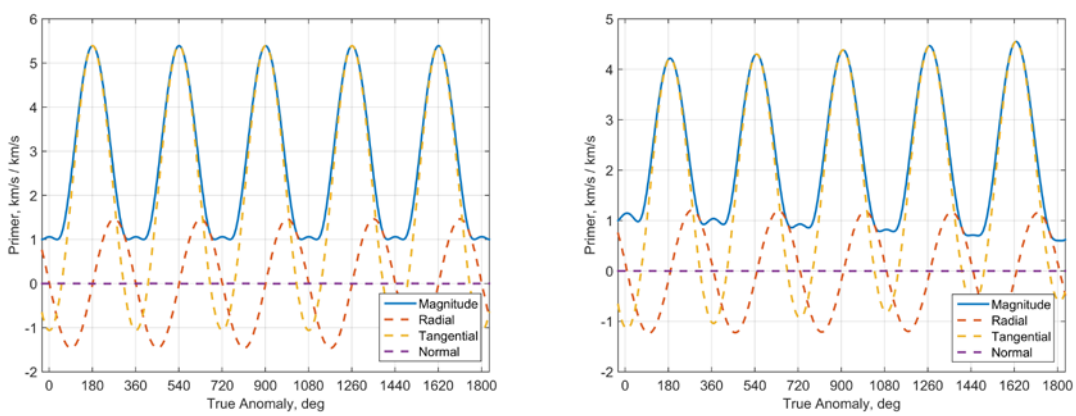

Figure 2 Primer vector behavior for pure leveraging (left) and capture (right) maneuvers of a near 6:5 moon:spacecraft resonance with Europa.

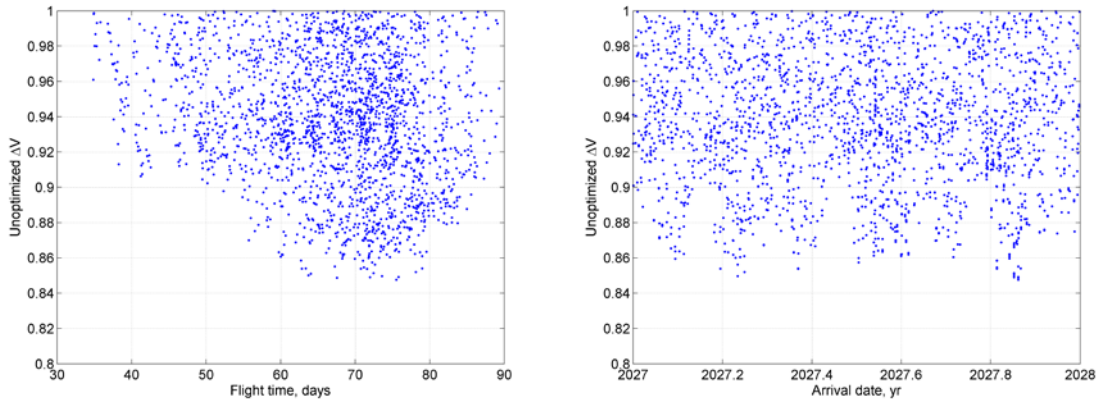

Figure 3 Broad search of flight time and arrival date to capture into 100 km circular orbit at Europa beginning with Callisto flyby.

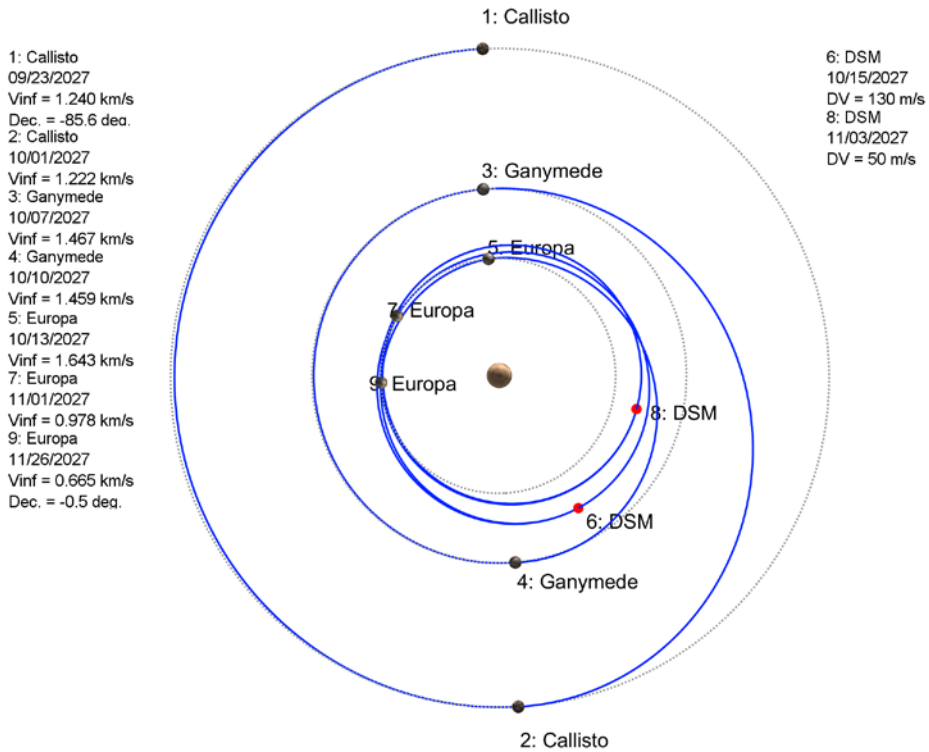

Figure 4 "Banzai Pipeline" trajectory[11] from broad search results with 64-day flight time and 870 m/s leveraging plus capture ΔV at Europa.

Saturn System Tour with Capture at Enceladus

The goal while designing a tour with relatively small moons of Saturn is not just to lower V_∞ for capture, but also to achieve the biggest change in orbital period to transfer between resonances. The tour begins with flybys of Titan, and works its way through shorter periods with flybys of Rhea, Dione, and Tethys to eventually capture into orbit at Enceladus. Because each successive flyby body has a shorter period than the previous, the objective is to minimize the period after the flyby at the end of the leg P_f^+ and maximize the period before the flyby at the beginning of each leg P_0^-. The period is computed from the Saturn-centered velocity v (before the beginning flyby and after the end flyby), radius of the flyby body r_B, and gravitational parameter of Saturn GM_S via Eq. (49).

$$J = P_f^+ - P_0^- \tag{48}$$

$$P = \frac{\pi GM_S}{\sqrt{2}}\left(\frac{GM_S}{r_B} - \frac{v^2}{2}\right)^{-3/2} \tag{49}$$

The velocity magnitudes are found by accounting for the maximum bending acheivable from each moon during the flyby. First, the angle α between the leg V_∞ (after the beginning flyby and before the end flyby) and the body velocity is found with Eq. (50). This angle is increased (with a maximum of π) to lower the period after the end flyby and decreased (with a minimum of 0) to increase the period before the beginning flyby on each leg by rotating through the maximum achivable flyby bending angle δ in Eq. (51). The Saturn-centered velocity before and after the flybys is then found from the new angle α' with Eq. (53).

$$\alpha = \cos^{-1}\left(\hat{\mathbf{v}}_\infty^T \hat{\mathbf{v}}_B\right) \tag{50}$$

$$\delta = 2\sin^{-1}\left[1\Big/\left(1 + r_{\min} v_\infty^2 / GM_B\right)\right] \tag{51}$$

$$\begin{aligned} \alpha_f'^+ &= \alpha_f^- + \delta \\ \alpha_0'^- &= \alpha_0^+ - \delta \end{aligned} \tag{52}$$

$$v^2 = v_B^2 + 2v_B v_\infty \cos\alpha' + v_\infty^2 \tag{53}$$

The primer vector over the transfer is then found from Eq. (18) using the partials of J with respect to the initial and final V_∞. An example for transfers over approximately four orbits of Rhea is presented in Figure 5. The optimal manevuer direction to change period using flybys is still tangential (as in the V_∞ leveraging case), but not necessarily at an apse. In fact the optimal location shifts from near periapsis to near apoapsis in Figure 6 as the flight time approaches 4:3 resonance with Rhea.

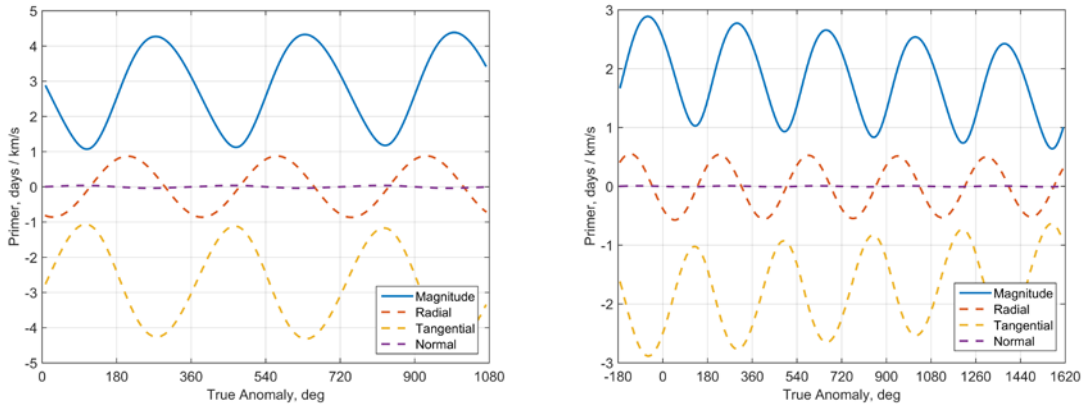

Figure 5 Primer vector magnitude and components to change orbital period for 17.85-day Rhea transfers. Left figure is near 4:3 moon:spacecraft resonance and right figure is near 4:5.

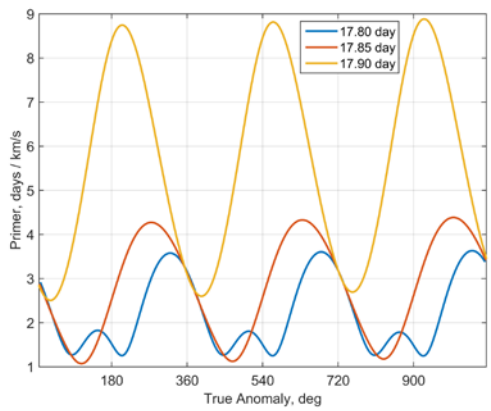

Figure 6 The effectiveness and optimal maneuver location for changing orbital period with gravity assists changes with flight time of the transfer.

A broad search of trajectories using maneuvers to change orbital period from Eq. (48) and to lower V_∞ from Eq. (47) is conducted using the design constraints in Table 2. The Pareto front of ΔV versus flight time from the broad search is shown in Figure 7, and the trajectories with minimum ΔV and minimum flight time are presented in Figure 8 and Figure 9. The tours along the Pareto front are similar up to the Enceladus encounters where the lower ΔV solution takes more time to circularize the orbit before orbit insertion.

Table 2. Search parameters to reduce capture ΔV into 100-km circular orbit at Europa

Maneuver Objectives	Reduce period or reduce V_∞
Max. maneuver ΔV	30 m/s Titan 40 m/s Rhea 20 m/s Dione 10 m/s Tethys 30 m/s Enceladus
Maneuver ΔV increment	3 m/s
Flyby Sequence	2–4 flybys of Titan 9–16 flybys of Rhea 6–11 flybys of Dione 7–13 flybys of Tethys 7–13 flybys of Enceladus
Initial conditions	1/1/2030 in 2:1 Titan resonance
Max. flight time per leg	40 days Titan 60 days Rhea 40 days Dione 30 days Tethys 30 days Enceladus
Max. spacecraft orbital revolutions per leg	5 Titan 15 Rhea 15 Dione 15 Tethys 20 Enceladus
Max. total flight time	3 yr
Time step	0.05 days Titan 0.03 days Rhea 0.02 days Dione 0.015 days Tethys 0.01 days Enceladus
Max. flyby ΔV	10 m/s
Min. flyby alt.	50 km

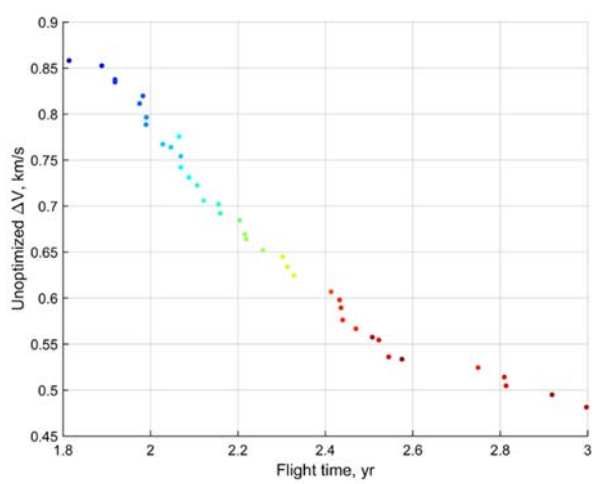

Figure 7 Pareto front of trajectories beginning in a 2:1 resonance with Titan and ending in circular orbit at Enceladus.

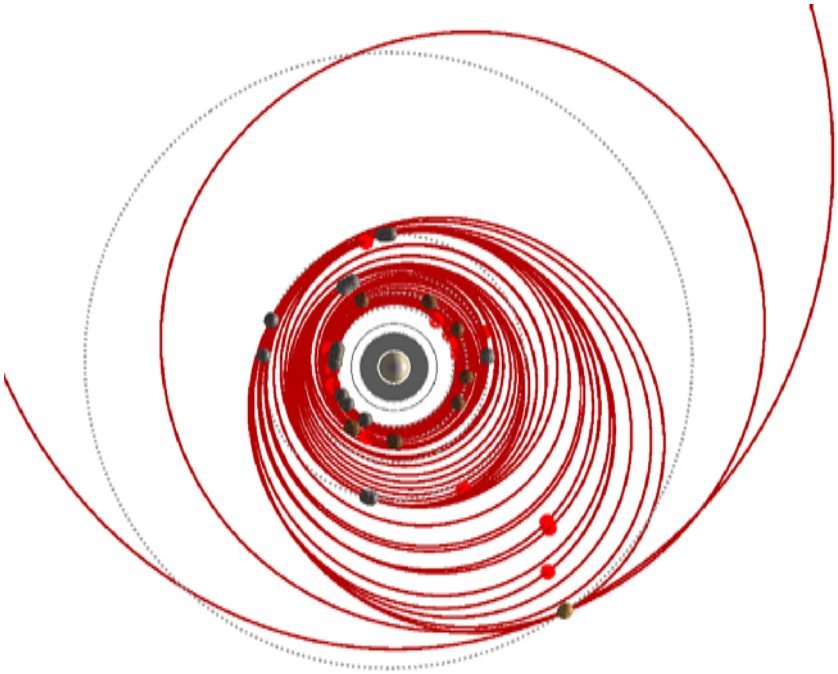

Figure 8 Minimum ΔV tour from broad search with 54 flybys.

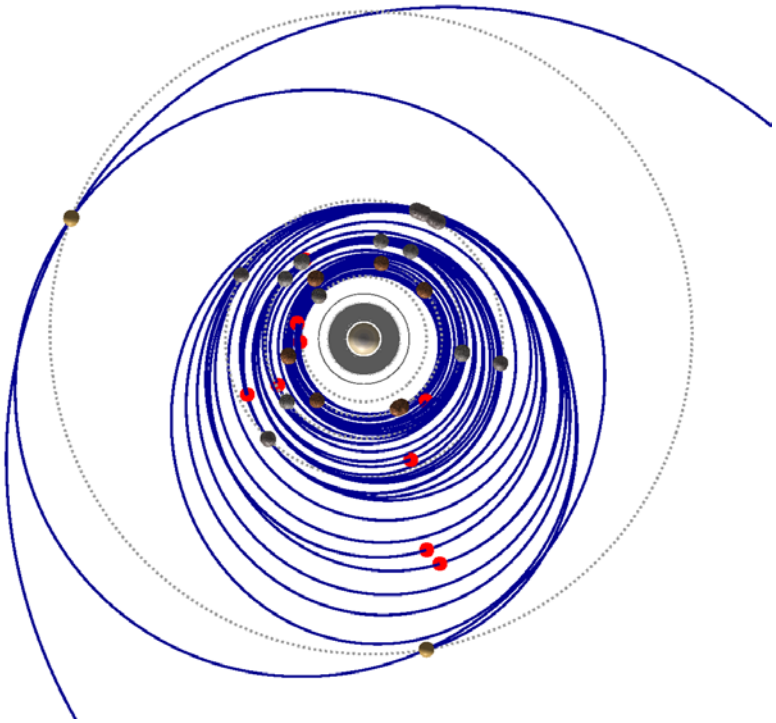

Figure 9 Minimum flight time tour from broad search with 36 flybys.

Broken Plane to Mars

The final example employs a fictitious launch vehicle with mass (in, say, tons) performance found in Eq. (54). The first term gives the effect of launch energy $C_3 = \mathbf{v}_\infty^T \mathbf{v}_\infty$ and the second term is included to give a mass penalty for launch declinations out of the equator, where $\hat{\mathbf{z}}$ is the direction of Earth's pole. The final "rocket equation" term accounts for the effect of a deep-space maneuver along the transfer. For this example, 900 s is used for the specific impulse I_{sp}.

$$J = \left(1 - 0.02C_3 + 0.0001C_3^2\right)\left(1 - \left|\hat{\mathbf{z}}^T \hat{\mathbf{v}}_\infty\right|\right) e^{-\Delta V / g I_{sp}} \tag{54}$$

A representative primer vector history is plotted in Figure 10, where the effect of the declination term introduces a strong sensitivity in the orbit-normal direction. The optimal time to perform the manevuer is found when the total magnitude is largest. Figure 11 illustrates a classic "broken plane" maneuver where the ballistic transfer is significantly out of plane, and a judiciously placed maneuver shifts the orbit to lower inclination. A broad search of trajectories to Mars using the fictitious launch vehicle is conducted with the search parameters of Table 3.

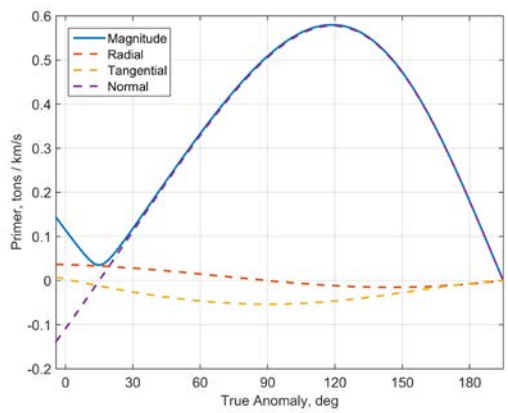

Figure 10 Primer vector over a representative transfer with objective from Eq. (54).

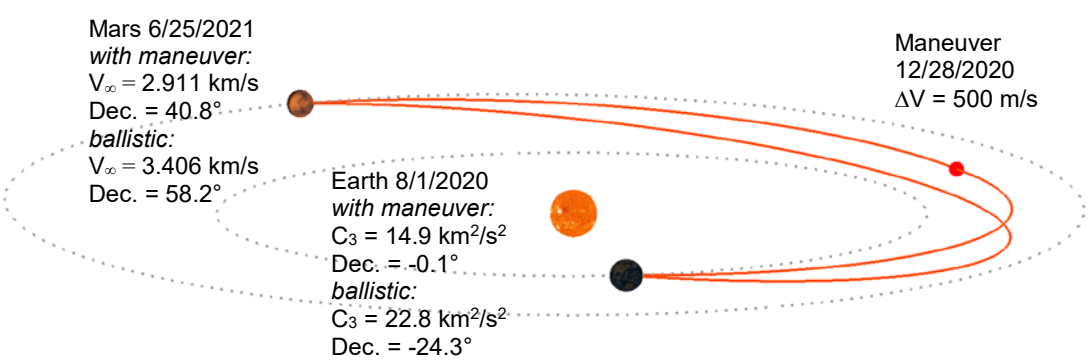

Figure 11 A deep-space maneuver normal to the ballistic orbit plane reduces C_3 and declination.

Table 3. Search parameters for maximum mass to Mars with Earth declination penalty

Maneuver Objective	Maximize mass
Max. maneuver ΔV	1,000 m/s
Maneuver ΔV increment	50 m/s
Launch range	2020–2053
Max. flight time	365 d
Time step	1 day
Max. V_∞	9 km/s

From Figure 12 the additional maneuver is shown to be able to fill in gaps of flight time where the ballistic transfers have either high C_3 or high delcination (or both). The valleys in the ballistic performance versus flight time (Figure 12, left) of are mainly due to the variation in performance over different launch opportunities (Figure 12, right). During the most favorable opportunities the difference in peak perfomance is less pronounced, but the additional manveuver can improve performance over a range of launch dates in a launch period as illustrated in Figure 13.

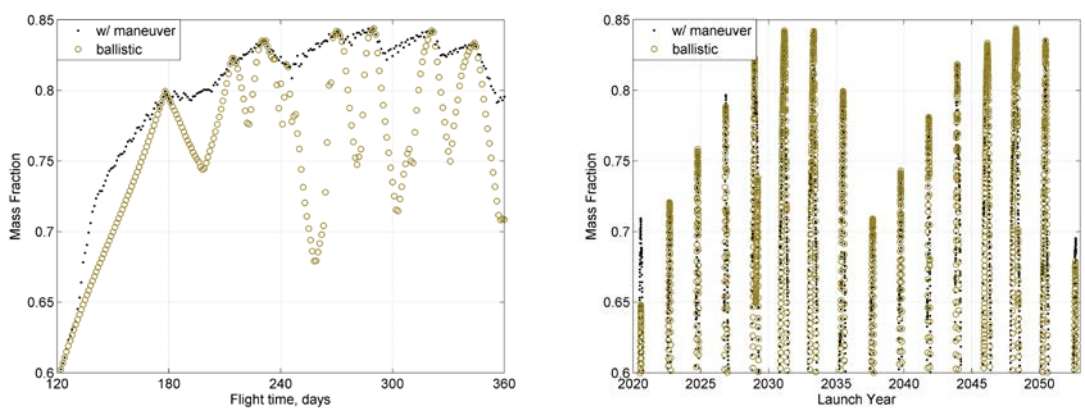

Figure 12 Pareto fronts of flight time over all launch dates and launch dates over all flight times.

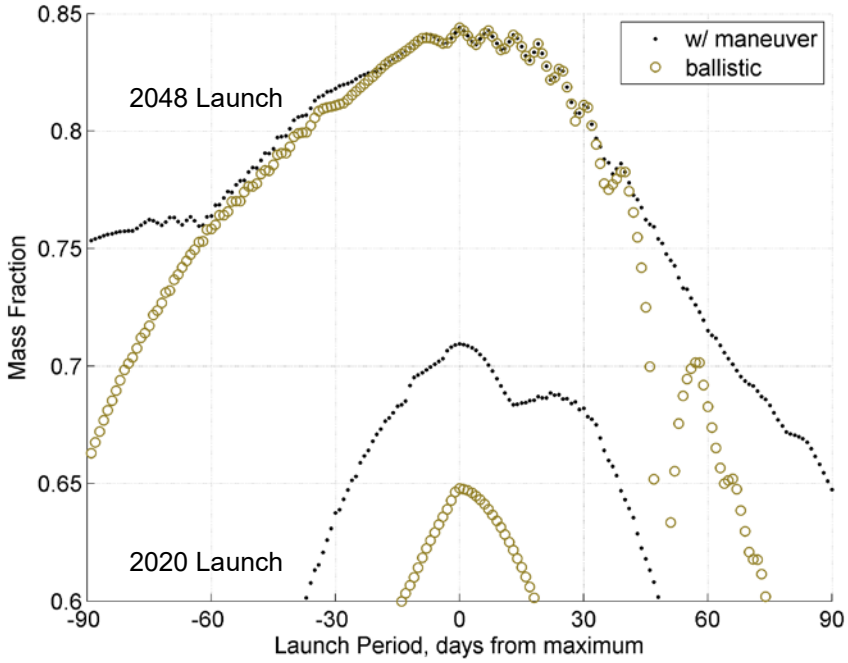

Figure 13 Launch periods for best and worst launch years.

CONCLUSIONS

It is possible to add maneuvers to automated trajectory searches without artificially constraining the maneuver or presupposing the mission objectives. Analysis of the Primer Vector specifies where and how a maneuver improves general mission objectives, and reduces the maneuver design down to two 1-dimensional searches from one 4-dimensional search per trajectory leg. The ΔV vector can be solved explicitly, leading to a 1-dimensional solve for flight time, similar to Lambert's problem. The resulting algorithm is computationally tractable and improves the results of automated broad search methods.

Acknowledgement

The author expresses his gratitude to Nitin Arora for testing the broad search code and uncovering so many bugs. He is also thankful to Kevin Scholtes for improving the trajectory plots. This research was carried out at the Jet Propulsion Laboratory, California Institute of Technology, under a contract with the National Aeronautics and Space Administration.

References

1. Izzo, D., Becerra, V. M., Myatt, D. R., Nasuto, S. J., and Bishop, J. M., "Search Space Pruning and Global Optimisation of Multiple Gravity Assist Spacecraft Trajectories," *Journal of Global Optimization*, Vol. 38, 2007, pp. 283–296.
2. Landau, D., Lam, T., and Strange, N.," Broad Search and Optimization of Solar Electric Propulsion Trajectories to Uranus and Neptune," AAS Paper 09-428, AAS/AIAA Astrodynamics Specialist Conference, Pittsburgh, PA, August 9–13, 2009.
3. Lantukh, D. V., Russell, R. P., and Campagnola, S., "Automated Inclusion of V-infinity Leveraging Maneuvers in Gravity-Assist Flyby Tour Design," AAS Paper 12-162.

4. Lawden, D. F., *Optimal Trajectories for Space Navigation*, Butterworths, London 1963.
5. Fernandes, S., "Note on the Solution of the Coast-Arc Problem," *Acta Astronautica*, Vol 45, No. 1, 1999, pp. 53–57.
6. Lawden, D. F., "Fundamentals of Space Navigation," *Journal of the British Interplanetary Society,"* Vol. 13, No 2, 1954, pp. 87–101.
7. Carter, T. E., "New Form for the Optimal Rendezvous Equations Near a Keplerian Orbit," *Journal of Guidance, Control, and Dynamics,"* Vol 13, No. 1, 1990, pp. 183–186.
8. Strange, N. J., Campagnola, S., and Russell, R. P., "Leveraging Flybys of Low Mass Moons to Enable an Enceladus Orbiter," AAS Paper 09-435.
9. Campagnola, S., Strange, N. J., and Russell, R. P., "A Fast Tour Design Method Using Non-Tangent V-Infinity Leveraging Transfer," *Celestial Mechanics and Dynamical Astronomy*, Vol 108, 2010, pp. 165–186.
10. Battin, R. H., *An Introduction to the Mathematics and Methods of Astrodynamics, Revised Edition*, American Institute of Aeronautics and Astronautics, Reston, VA, 1999.
11. McElrath, T. P., Campagnola, S., and Strange, N., "Riding the Banzai Pipeline at Jupiter: Balancing Low ΔV and low Radiation to Reach Europa," AIAA Paper 2012-4809.